Geoderma 467 (2026) 117719

Contents lists available at ScienceDirect

Geoderma

journal homepage: www.elsevier.com/locate/geoderma

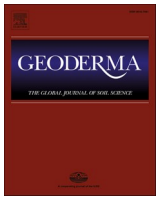

Intensive smooth cordgrass removal strengthens tidal and temperature impacts on methane emission☆

Yueting Deng [a,b,c,d], Ruichen Lin [a,b,c,d], Han Yang [a,b,c,e], Hui Luo [b,d], Lulu Song [f,*], Xudong Zhu [a,b,c,d,e,*]

[a] State Key Laboratory of Marine Environmental Science, Xiamen University, Xiamen, Fujian, China
[b] National Observation and Research Station for the Taiwan Strait Marine Ecosystem (Xiamen University), Zhangzhou, Fujian, China
[c] Key Laboratory of the Coastal and Wetland Ecosystems (Ministry of Education), Xiamen University, Xiamen, Fujian, China
[d] College of the Environment and Ecology, Xiamen University, Xiamen, Fujian, China
[e] Coastal and Ocean Management Institute, Xiamen University, Xiamen, Fujian, China
[f] State Key Laboratory for Ecological Security of Regions and Cities, Institute of Urban Environment, Chinese Academy of Sciences, Xiamen, Fujian, China

ARTICLE INFO

Keywords:
Spartina alterniflora
Eddy covariance
Restoration
Diel variability
Blue carbon

ABSTRACT

The world's largest ecosystem restoration via intensive removals of invasive smooth cordgrass (*Spartina alterniflora*) is being implemented in coastal China, potentially exerting a large impact on soil biogeochemical cycles of greenhouse gases including methane (CH_4). However, the degree to which CH_4 emission and its environmental controls change with such anthropogenic disturbances has been rarely assessed with direct empirical evidence. To quantify these disturbance effects, we utilized the eddy covariance (EC) approach to continuously measure net CH_4 exchange from Jul. 2022 to Oct. 2023, covering both pre- and post-removal periods, in a disturbed coastal wetland of Southeast China experiencing an intensive cordgrass removal in late Oct. 2022. Our analyses, based on this unique EC dataset of high-frequency (30-min) time series CH_4 fluxes, revealed that (a) the removal caused a pulse of CH_4 emission peaking one month later up to 0.76 g CH_4 m^{-2} d^{-1}, with the mean post-removal emission over ten times that of the pre-removal level (0.03 g CH_4 m^{-2} d^{-1}); (b) the removal intensified the controls of tidal inundation and pumping on CH_4 fluxes, showing much stronger pumping effects within two months following the disturbances; (c) the removal also enlarged the temperature sensitivity of CH_4 emission, leading to larger daytime emission especially at afternoon hours; (d) the combination of enhanced tidal impacts and temperature dependence thus promoted the diel variability of CH_4 fluxes during the post-removal period. These results suggest that coastal restoration via intensive cordgrass removals boosts both the magnitude and the diel variability of CH_4 emission, highlighting the necessity of better understanding the climate impact of restoration activities. Future longer flux data with extended years are needed to further assess potential regime shift in soil CH_4 biogeochemistry and long-term evolution of such unintended environmental costs of the restoration.

1. Introduction

As a cost-effective natural solution for mitigating climate change, coastal blue carbon ecosystems (BCEs) have attracted significant attentions due to their efficient carbon sequestration capacity (Macreadie et al., 2021; Wang et al., 2023a). BCEs can reduce approximately 304 Tg carbon dioxide (CO_2) emission annually (Macreadie et al., 2021). However, as hotspots of biogeochemical cycling of greenhouse gases (GHGs), they also emit 0.47–1.41 Tg methane (CH_4) annually (Rosentreter et al., 2023), significantly offsetting their carbon sequestration benefits (Rosentreter et al., 2018). Unfortunately, the contribution of CH_4 emission is often overlooked in current blue carbon assessments. More critically, factors such as biological invasions, anthropogenic land-use change, and climate change are accelerating the degradation of BCEs (Macreadie et al., 2021). As one of the world's most threatened habitats, BCEs are being lost at an annual rate of 0.13–1.5%, resulting in annual emission of 0.15–1.02 Pg CO_2 and severely compromising their carbon sequestration potential (Fu et al., 2024). In response to the United Nations Decade on Ecosystem Restoration, urgent and effective measures must be taken to enhance the protection and

☆ This article is part of a special issue entitled: 'Soil Methane Biogeochemistry' published in Geoderma.

* Corresponding authors.
E-mail addresses: llsong@iue.ac.cn (L. Song), xdzhu@xmu.edu.cn (X. Zhu).

https://doi.org/10.1016/j.geoderma.2026.117719
Received 29 October 2025; Received in revised form 4 January 2026; Accepted 3 February 2026

restoration of BCEs, maximizing their carbon sequestration capacity and ecosystem service benefits.

China occupies one of the most severely degraded coastal zones in the world, and has implemented systematic ecological restoration measures (e.g., invasive species removal and habitat reconstruction) to strengthen the protection of BCEs (Liu et al., 2016). Originally native to the Atlantic coast of the United States, smooth cordgrass (*Spartina alterniflora*) has spread rapidly since its introduction to China in 1979 and occupies over 60% of the country's total saltmarsh area along the coastline (Nie et al., 2023). Recently, the Chinese government launched a large-scale removal campaign in 2022, aiming to eliminate 90% of the invasive cordgrass by 2025 (Stokstad, 2023; Xie and Han, 2023). Recent studies have primarily used scenario analyses to assess the long-term ecological benefits of this campaign (Qi et al., 2024; Yang et al., 2024), but insufficient attention has been paid to the short-term ecological effects of such intensive anthropogenic disturbances. In fact, wetland ecosystems are highly sensitive to anthropogenic disturbances (He et al., 2025). Human-induced land use and land cover changes can significantly alter wetland landscape patterns, thereby affecting their carbon storage capacity and GHG emission characteristics (Sasmito et al., 2019). Such disturbances may lead to a regime shift in the ecosystem's carbon sink pattern, e.g., the disturbances transformed the ecosystem from a stable CO_2 sink into a weak source (Zhu et al., 2024b). The removal and burial of cordgrass may lead to intensive decomposition and decay of residual biomass, potentially releasing substantial amounts of GHGs (Yang et al 2024) with short-term pulse emission (Pendleton et al., 2012). However, there is still a lack of accurate quantification and estimation of GHG fluxes via direct empirical data, especially the CH_4 fluxes before and after the cordgrass removal.

In BCEs, CH_4 emission primarily originates from the microbial decomposition of soil organic matter, with the availability of organic substrates often being a key limiting factor for CH_4 production (Al-Haj and Fulweiler., 2020; Noyce and Megonigal, 2021; Hu et al., 2024). Notably, anthropogenic disturbances can trigger pulse GHG emission, typically associated with the short-term input of large amounts of organic matter and the rapid decomposition of labile substrates. For example, it has been shown that the mortality of belowground biomass in disturbed mangroves provides abundant substrates for microbial decomposition, significantly enhancing heterotrophic respiration and substantially increasing CO_2 emission (Sasmito et al., 2019). The ultimate CH_4 efflux entering the atmosphere is the result of multiple biogeochemical processes, including CH_4 production, oxidation, and transport (Bridgham et al., 2013). These complex processes are jointly regulated by various environmental factors, among which temperature plays a particularly prominent role. It is widely recognized that temperature directly and indirectly controls soil biogeochemical processes by modulating microbial metabolism and influencing substrate availability (Wang et al., 2015). Higher temperature not only significantly enhances the metabolic activity of methanogens but also accelerates organic matter decomposition, thereby providing more abundant substrates for CH_4 production (Hu et al., 2020). Emerging research further reveals that the temperature sensitivity of CH_4 emission may be closely linked to the decomposability of carbon substrates (Hu et al., 2024). Tidal activity represents another critical physical process influencing CH_4 fluxes. On the one hand, the changes in water table caused by tidal activities can affect CH_4 production and oxidation via altering oxygen availability (Hu et al., 2024), or modulate CH_4 release through hydrostatic pressure adjustments and tidal pumping effects (Wei et al., 2020; Cui et al., 2024; Zhu et al., 2024a). On the other hand, lateral tidal flows may introduce allochthonous organic carbon, promoting CH_4 production (Cui et al., 2024), while simultaneously facilitating the lateral export of sequestered blue carbon (Wang et al., 2023a). These intricate regulatory mechanisms with the interactions among various factors may amplify anthropogenic impacts on CH_4 fluxes, resulting in significant temporal variability in CH_4 emission from BCEs.

The changes in CH_4 flux dynamics induced by anthropogenic disturbances from coastal restorations remain a critical knowledge gap in blue carbon science (Macreadie et al., 2021). To date, the degree to which CH_4 emission and its environmental controls changes with disturbance in BCEs has been rarely assessed with direct empirical evidence. A major constraint is the lack of sufficient CH_4 flux measurements with a high temporal resolution. The application of eddy covariance (EC) technique, capable of measuring high-frequency and continuous GHG fluxes between ecosystems and the atmosphere (Baldocchi, 2020; Zhang et al., 2022; Zhang et al., 2023; Deng et al., 2025), could serve as an efficient approach to help close this knowledge gap.

Here, to quantify these disturbance effects on CH_4 flux dynamics, we utilized the EC approach to continuously measure CH_4 flux from Jul. 2022 to Oct. 2023, covering both pre- and post-removal periods, in a disturbed saltmarsh-mangrove wetland of Southeast China experiencing an intensive cordgrass removal in late Oct. 2022. Specific objectives are (1) to quantitatively compare the differences in the temporal variability of CH_4 fluxes before and after the cordgrass removal, and (2) to assess the potential change in the response of CH_4 fluxes to key environmental controls including tidal activities and temperature dependence. We hypothesize that coastal restoration via intensive smooth cordgrass removal strengthens tidal and temperature impacts and thus promotes the magnitude of CH_4 emission and its diel variability (Fig. 1). This study should offer direct empirical evidence to improve the understanding of the effects of restoration-induced anthropogenic disturbances on the temporal variability and environmental controls of CH_4 emission.

2. Materials and methods

2.1. Study area

A flux tower (23.9201°N, 117.4227°E; part of ChinaFLUX and USCCC) was established in a disturbed tidal wetland experiencing cordgrass removals, within Zhangjiang Mangrove National Nature Reserve in Southeast China, to conduct EC measurements of net CH_4 exchange (NME) between the wetland and the atmosphere (Zhu et al., 2021c). This wetland has a subtropical monsoon climate, with a mean air temperature of 21.1℃ and annual rainfall of 1165.5 mm, and experiences a semidiurnal tidal regime, with a mean tidal range of 2.1 m and surface water salinity of 12.6 ppt (Lu and Zhu, 2021; Zhu et al., 2019a; Zhu et al., 2021b). This wetland has experienced range expansions of both invasive cordgrass and native mangroves over the past decade to form a saltmarsh-mangrove ecotone (Fig. 1a) (Zhu et al., 2019b; Zhu et al., 2024b). Since late Oct. 2022, the government initiated a large-scale coastal wetland restoration effort to intensively remove cordgrass and thus turned the ecotone into a mudflat-mangrove habitat (Fig. 1b) within a few weeks (Zhu et al., 2025). Successive removal campaigns were maintained to prevent the cordgrass regrowth, including a moderate one occurring in late Jun. 2023. According to the detailed removal activities revealed by in-situ camera monitoring (Zhu et al., 2024b), we defined a pre-removal period from Jul. 8th, 2022 to Oct. 20th, 2022 and a post-removal period from Nov. 1st, 2022 to Oct. 31st, 2023.

2.2. Field measurements

The 30-min NME time series data were derived from raw 10-Hz measurements by an open-path EC system of a three-axis anemometer (CSAT-3, Campbell Scientific, Inc., Logan, UT, USA) and a CH_4 gas analyzer (Li-7700, Li-COR Inc., Lincoln, NE, USA). The 10-Hz data were processed into 30-min data following a series of flux correction (e.g., axis rotation, frequency response, ultrasonic, and WPL corrections) and quality control (e.g., steady state, turbulent condition, statistical, and absolute limit tests) processes, as implemented in the EddyPro software (Li-COR Inc.) (Zhu et al., 2019c; Zhu et al., 2021a; Liu and Zhu, 2024). The flux data quality was labeled using the 0–1–2 flagging system (Mauder et al., 2013), and the data with a quality flag of 2 were excluded

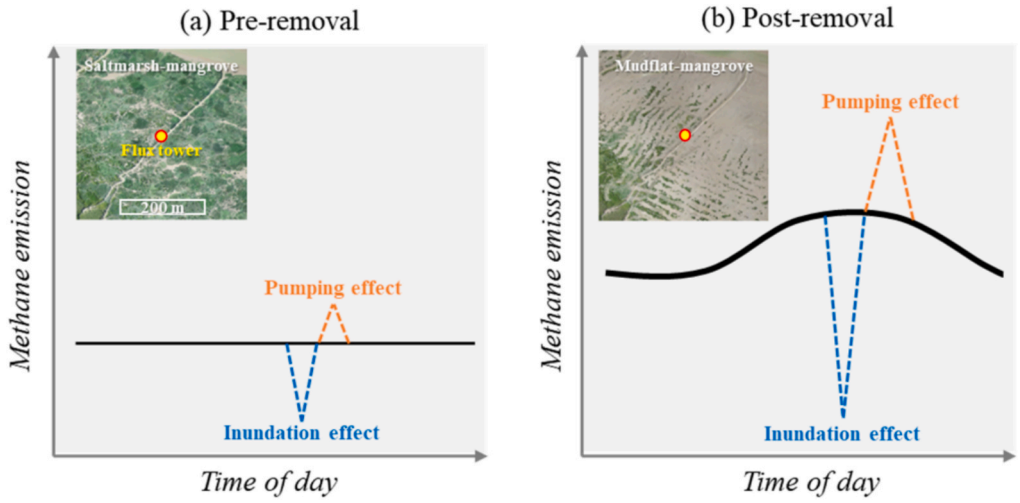

Fig. 1. Conceptual diagram illustrating the changes in methane emission and its diel variability along with the smooth cordgrass removal in a disturbed tidal wetland. Wetland landscape around the flux tower during the (a) pre-removal (saltmarsh-mangrove habitat) and (b) post-removal (mudflat-mangrove habitat) periods are shown by two insets of drone mosaic images acquired in Jun. 2022 and Jul. 2023, respectively. Tidal inundation and pumping are expected to suppress and promote methane emission, respectively.

from further analyses (Zhu et al., 2021a; Wang and Zhu, 2024). Additionally, flux data under conditions of rainfall and insufficient nighttime turbulence were also excluded (Zhu et al., 2021c). Regular system maintenance (e.g., manually cleaning Li-7700 mirrors) was conducted to ensure the data quality and the NME data with signal strength below 20% were excluded (Zhu et al., 2021c). Footprint climatology analyses confirmed that 80% of the fluxes were contributed from the habitats within ~ 200 m around the tower, dominated by southeast and northwest wind directions (Zhu et al., 2024b). As a result of quality controls and system malfunctions, the coverage of valid 30-min NME data was 62.9% (66.2% for daytime and 59.5% for nighttime) over the study period from Jul. 8th, 2022 to Oct. 31st, 2023. Auxiliary 30-min meteorological and tidal data included photosynthetically active radiation (PAR; PQS1 PAR Quantum sensor, Kipp & Zonen, Delft, Netherlands), air temperature (Tair; HMP155A sensor, Vaisala, Helsinki, Finland), rainfall (TE525MM Rain Gage, Campbell Scientific, Inc.), and surface water level (HOBO U20L-04 Water Level Logger, Onset, Bourne, MA, USA).

2.3. Data analyses

The 30-min NME data were temporally aggregated to daily data. To ensure a minimum representative coverage of the diel cycle while retaining a sufficient number of days for analysis, the days with daytime valid 30-min records below one-fourth or nighttime valid records below one-eighth were excluded from the temporal aggregation. A solar elevation angle threshold of zero was applied to distinguish daytime and nighttime periods. To reduce the effect of the uneven data missing issue, the mean NME was calculated separately for daytime and nighttime and then temporally aggregated to daily data. Daily data were further averaged to monthly data. Over the studying period, the percentage of valid daily NME was 77.3%. To examine the difference in NME between daytime and nighttime, we used an independent *t*-test analysis to statistically compare daytime and nighttime 30-min NME for each month over the studying period. Pearson correlation analyses were used to examine the correlations among 30-min NME and relevant environmental variables for both pre- and post-removal periods. To examine the tidal impacts on NME, mean diel variation (MDV) analyses were conducted to compare the diel variability of NME under tidal inundated and exposed conditions. To explore the correlation between air temperature and NME, Pearson correlation coefficients were also calculated between 30-min NME and air temperature for each single day. To better examine the change in the temperature dependence of NME over time, we quantified the temperature sensitivity of Q_{10} for each month. The NME data acquired under tidal exposed conditions were used only to avoid the confounding effect of tidal inundation. Specifically, all 30-min NME data under tidal exposed conditions for each month were bin averaged into 10 groups by the percentiles of air temperature and then the exponential equation with parameters a and b (Eq. (1); Wang et al., 2015) was used to fit the empirical relationship between temperature percentiles (T) and binned median NME. Thus, monthly Q_{10} was calculated from the fitted parameter b (Eq. (2)).

$$NME = a \bullet exp^{b \bullet T} \quad (1)$$

$$Q_{10} = exp^{10b} \quad (2)$$

In this study, a positive (negative) NME value indicated an upward (downward) CH_4 flux or a CH_4 source (sink). All data processing and statistical analyses were performed in MATLAB software (MathWorks Inc., Natick, MA, USA).

3. Results

3.1. Temporal variations in methane emission

Over the pre-removal period, daily NME varied from 0.008 g CH_4 m^{-2} d^{-1} to 0.067 g CH_4 m^{-2} d^{-1} and monthly mean NME changed from 0.018 ± 0.003 (mean ± std.) g CH_4 m^{-2} d^{-1} in Oct. 2022 (excluding the end of month during the removal period) to 0.034 ± 0.009 g CH_4 m^{-2} d^{-1} in Aug. 2022 (Fig. 2a). The removals significantly boosted the emission with pulse increases following each of the two major removals (intensive and moderate ones). The peak emission of the first pulse approximately one month later (0.764 g CH_4 m^{-2} d^{-1}) was 27.3 times that of the pre-removal level (0.028 ± 0.008 g CH_4 m^{-2} d^{-1}), while the peak emission of the second pulse (0.596 g CH_4 m^{-2} d^{-1}) was twice that of the previous month (0.301 ± 0.034 g CH_4 m^{-2} d^{-1}). Over the post-removal period, the two highest mean monthly NME occurred in the month right after each of the two major removals (0.530 g CH_4 m^{-2} d^{-1} in Nov. 2022 and 0.496 g CH_4 m^{-2} d^{-1} in Jul. 2023), while the lowest mean monthly NME of 0.146 g CH_4 m^{-2} d^{-1} occurred in Mar. 2023. Mean daily NME over the full post-removal period (0.297 ± 0.155 g CH_4 m^{-2} d^{-1}) was 10.6 times that of the pre-removal level. The direct comparison of NME for the same time window (Jul. 8th ~ Oct. 20th) with available measurements both before and after the removal indicated that the post-removal mean

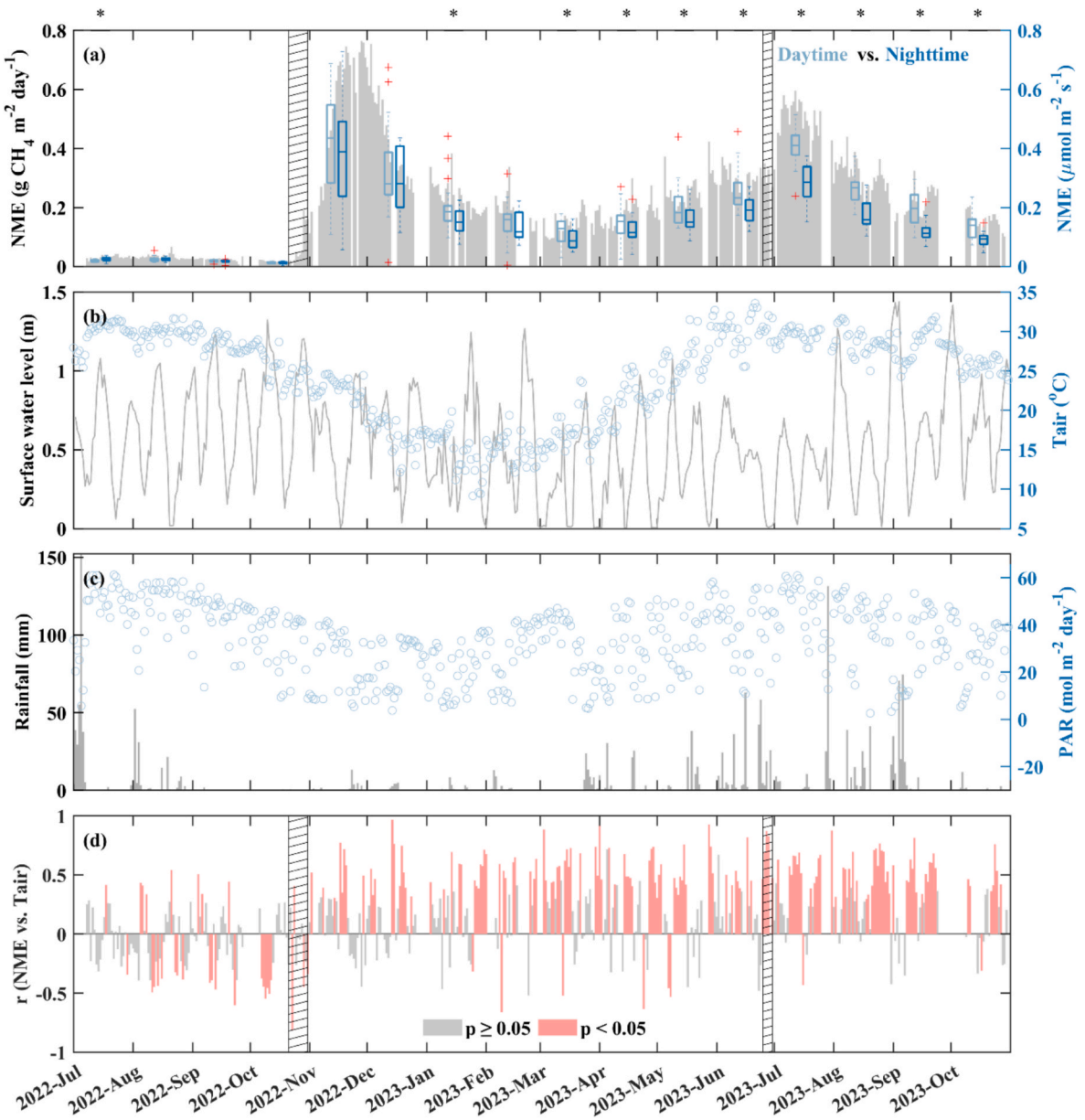

Fig. 2. Temporal variability of methane emission and environmental factors from Jul. 2022 to Oct. 2023 in a disturbed tidal wetland experiencing smooth cordgrass removals, including (a) daily/monthly net methane exchange (NME), (b) daily maximum surface water level, daily mean air temperature (Tair), (c) daily rainfall, and daily photosynthetically active radiation (PAR). The differences in 30-min NME between daytime (light blue) and nighttime (dark blue) periods for each month are shown by a pair of boxplots, with an asterisk above the upper x-axis indicating a statistical significance ($p < 0.05$) (a). Daily Pearson correlation coefficients (r) between 30-min NME and Tair are shown with statistically significant (red) and non-significant (gray) values (d). The two diagonal shadings indicate the intensive (late Oct. 2022) and moderate (late Jun. 2023) removals, respectively (a and d).

daily NME (0.317 ± 0.128 g CH_4 m^{-2} d^{-1}) was 11.3 times higher than the pre-removal level (Fig S1). Overall, CH_4 emission increased significantly following the intensive removal, sustaining a pulse emission for approximately two months before a winter decline. Thereafter, emission rebounded from the beginning of the growing season (Mar. 2023) onward until the moderate removal event triggering another emission pulse, after which a sustained decreasing trend was observed.

Over the pre-removal period, no statistically significant difference (*t*-test) was observed between daytime and nighttime NME except Jul. 2022 (Fig. 2a). Monthly-mean daytime NME ranged from 0.018 ± 0.004 μmol·m^{-2} s^{-1} in Sep. 2022 to 0.024 ± 0.008 μmol·m^{-2} s^{-1} in Aug. 2022, while nighttime NME varied between 0.012 ± 0.004 μmol·m^{-2} s^{-1} in Oct. 2022 (excluding the end of month during the removal period) and 0.025 ± 0.006 μmol·m^{-2} s^{-1} in Aug. 2022, with a diel difference (i.e., daytime minus nighttime) of −0.004–0.0008 μmol·m^{-2} s^{-1}. In the month following the intensive removal (Nov. 2022), mean daytime and nighttime NME increased to 0.426 ± 0.170 μmol·m^{-2} s^{-1} (34.5 times that of Oct. 2022) and 0.379 ± 0.175 μmol·m^{-2} s^{-1} (31.2 times), respectively. Over the post-removal period, the mean daytime NME of 0.237 ± 0.131 μmol·m^{-2} s^{-1} (nighttime: 0.187 ± 0.112 μmol·m^{-2} s^{-1}) was 11.9 (8.9) times that of the pre-removal daytime level of 0.020 ± 0.007 μmol·m^{-2} s^{-1} (0.021 ± 0.007 μmol·m^{-2} s^{-1}). The lowest post-removal NME in Mar. 2023 (daytime: 0.118 ± 0.041 μmol·m^{-2} s^{-1}; nighttime: 0.091 ± 0.031 μmol·m^{-2} s^{-1}) were still 5.9 and 4.3 times that of the pre-removal levels, respectively. *T*-test statistical analyses confirmed that daytime NME was statistically significantly larger than nighttime NME in most months over the post-removal period. These diel differences were further revealed by the monthly MDV analyses (Fig. 3).

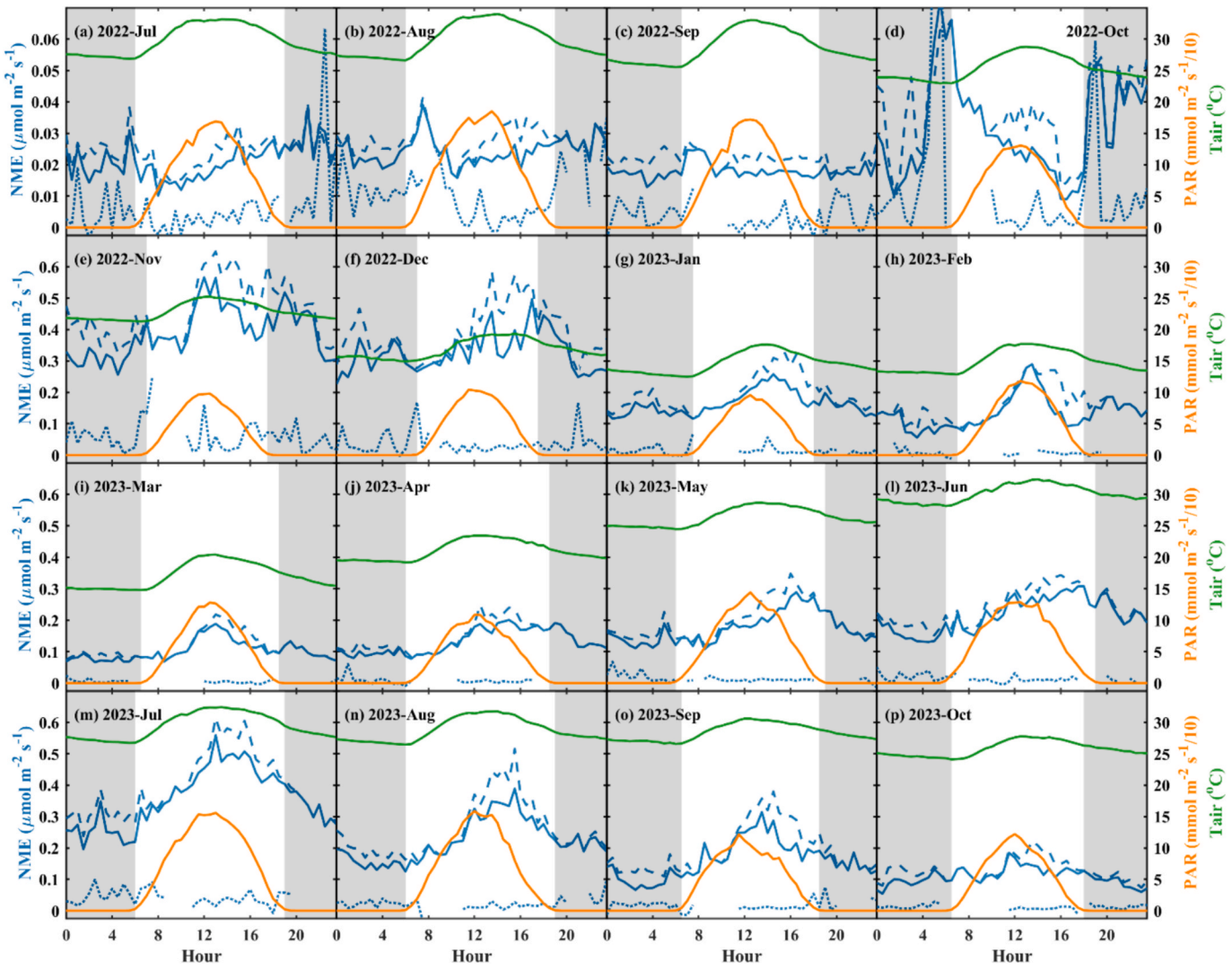

Fig. 3. Mean diel variations in 30-min net methane exchange (NME; blue), photosynthetically active radiation (PAR; orange), and air temperature (Tair; green) for each month from Jul. 2022 to Oct. 2023. Mean diel variations in 30-min NME under tidal exposed (dashed blue) and inundated (dotted blue) conditions are also shown for each month. Note that the scale of NME used for the first row was different from that for the other rows.

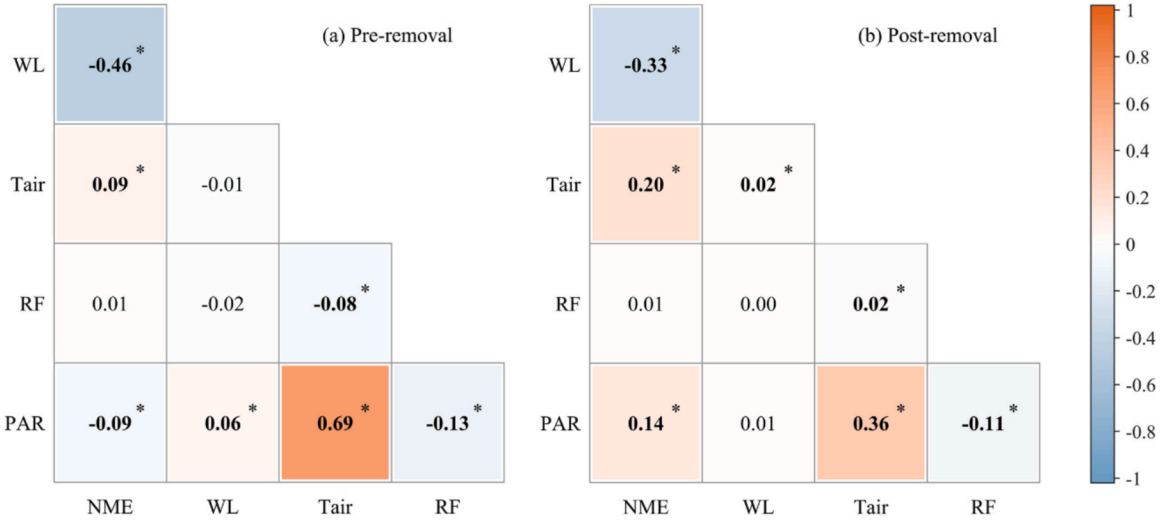

Fig. 4. Heatmaps of Pearson correlation coefficients during the pre-removal (a) and post-removal (b) periods among 30-min net methane exchange (NME) and environmental factors, including surface water level (WL), air temperature (Tair), rainfall (RF), and photosynthetically active radiation (PAR). Statistically significant ($p < 0.05$) coefficients are in bold and marked with asterisks.

Over the pre-removal period, NME was relatively constant over the course of a day without obvious diel differences, while over the post-removal period NME had much stronger diel variability with higher daytime emission occurring in the afternoon.

3.2. Environmental controls on methane emission

Potential environmental controls on CH_4 emission were explored using Pearson correlation analyses between 30-min NME and environmental factors (Fig. 4). Over the pre-removal period, 30-min NME was statistically significantly ($p < 0.05$) correlated with WL (correlation coefficient: −0.46), Tair (0.09) and PAR (−0.09), while its correlation with RF (0.01) was not statistically significant. Over the post-removal period, 30-min NME was also statistically significantly correlated with WL (−0.33), Tair (0.20) and PAR (0.14). Given that both pre- and post-removal NME were statistically significantly correlated with WL and Tair on a 30-min scale, we further examined tidal and temperature impacts on NME on a sub-daily scale. Based on the monthly MDV analyses, CH_4 emission under inundated conditions was obviously lower than that under exposed conditions (Fig. 3). Over the pre-removal period, mean NME under inundated conditions ranged from 0.003 to 0.013 μmol·m^{-2} s^{-1}, while mean NME under exposed conditions was 2.6–6.5 times higher, ranging from 0.022 to 0.037 μmol·m^{-2} s^{-1}. Over the post-removal period, mean NME under inundated conditions varied from 0.006 to 0.059 μmol·m^{-2} s^{-1}, while mean NME under exposed conditions was 9.0–27.0 times higher, ranging from 0.114 to 0.456 μmol·m^{-2} s^{-1}. Based on the 30-min time series of NME, pronounced tidal pumping effects were well identified, in which the efflux surged abruptly at the transition from inundated to exposed conditions (Fig. 5). This pumping effect was obviously stronger during the two months following the removal events. Direct comparison of 30-min NME before and after the inundation-exposure transition indicated that, over the pre-removal period, the efflux right after the transition was 2.0–3.4 times higher, while this difference increased to 4.6–9.9 times over the post-removal period.

Although pulse emissions occurred after the removal, the seasonal variability of CH_4 efflux underlying the pulse emissions still matched the seasonal pattern of Tair (Fig. 2a-b). Nearly half (48.9%) of valid days showed statistically significant correlations between 30-min NME and Ta over the post-removal period, while there was only 27.1% over the pre-removal period (Fig. 2d). Pearson correlation coefficients over the post-removal period were overall higher than those over the pre-removal period. Over the pre-removal period, weak temperature dependence of NME was observed with monthly Q_{10} close to one (1.01–1.13), while over the post-removal period, the temperature dependence obviously increased with Q_{10} varying from 1.46 in Nov. 2022 to 3.30 in Feb. 2023 (Fig. 6). On average, the post-removal Q_{10} values were 2.39 times that of the pre-removal level. By comparing the

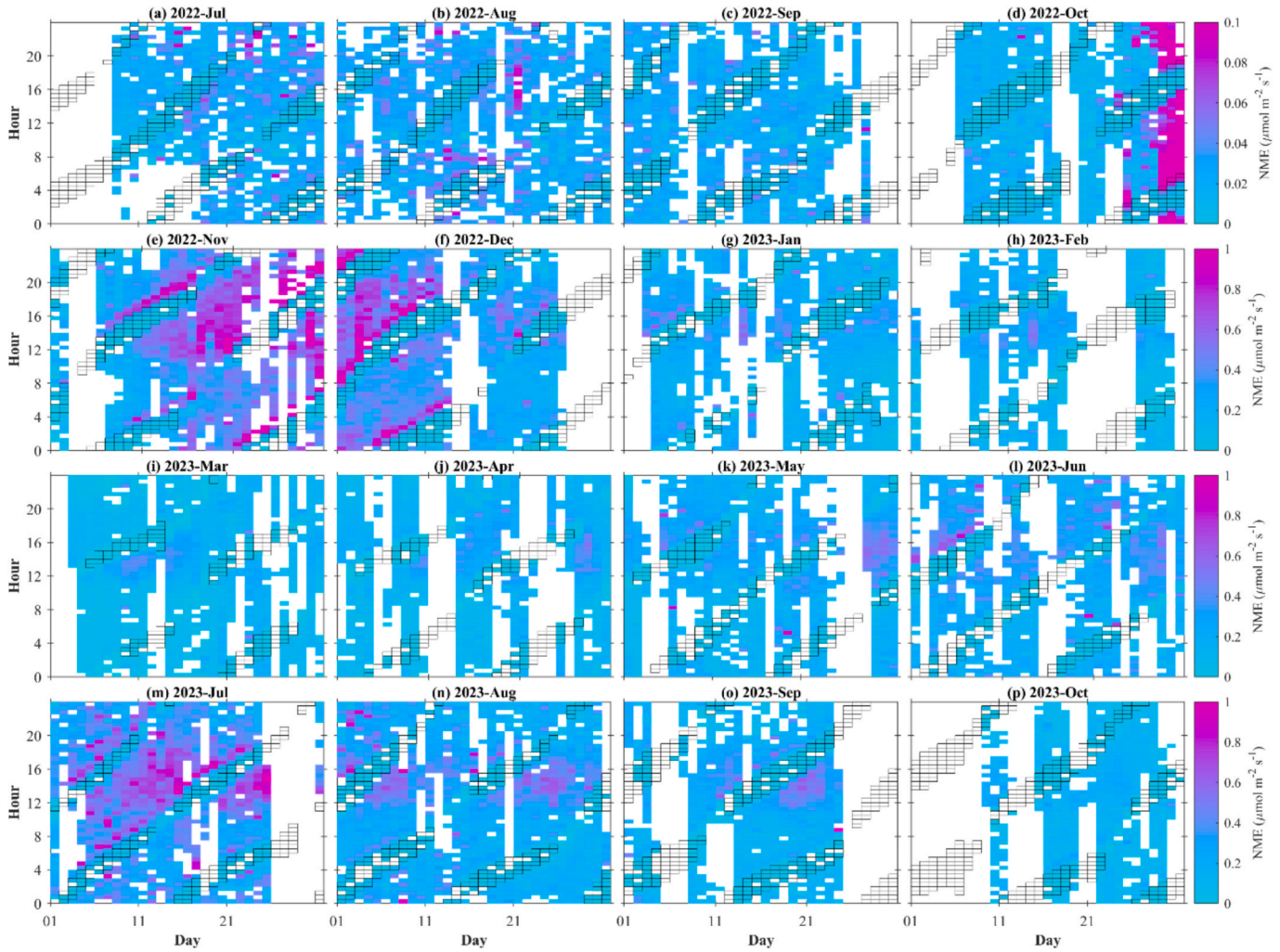

Fig. 5. Temporal variability of 30-min net methane exchange (NME) in a disturbed tidal wetland experiencing smooth cordgrass removals for each month from Jul. 2022 to Oct. 2023. The grids with a black outline indicate those 30-min periods experiencing tidal inundation. Note that the rightmost color bar applies to the four months in the same row, with the first row using different scales from the others for better visibility.

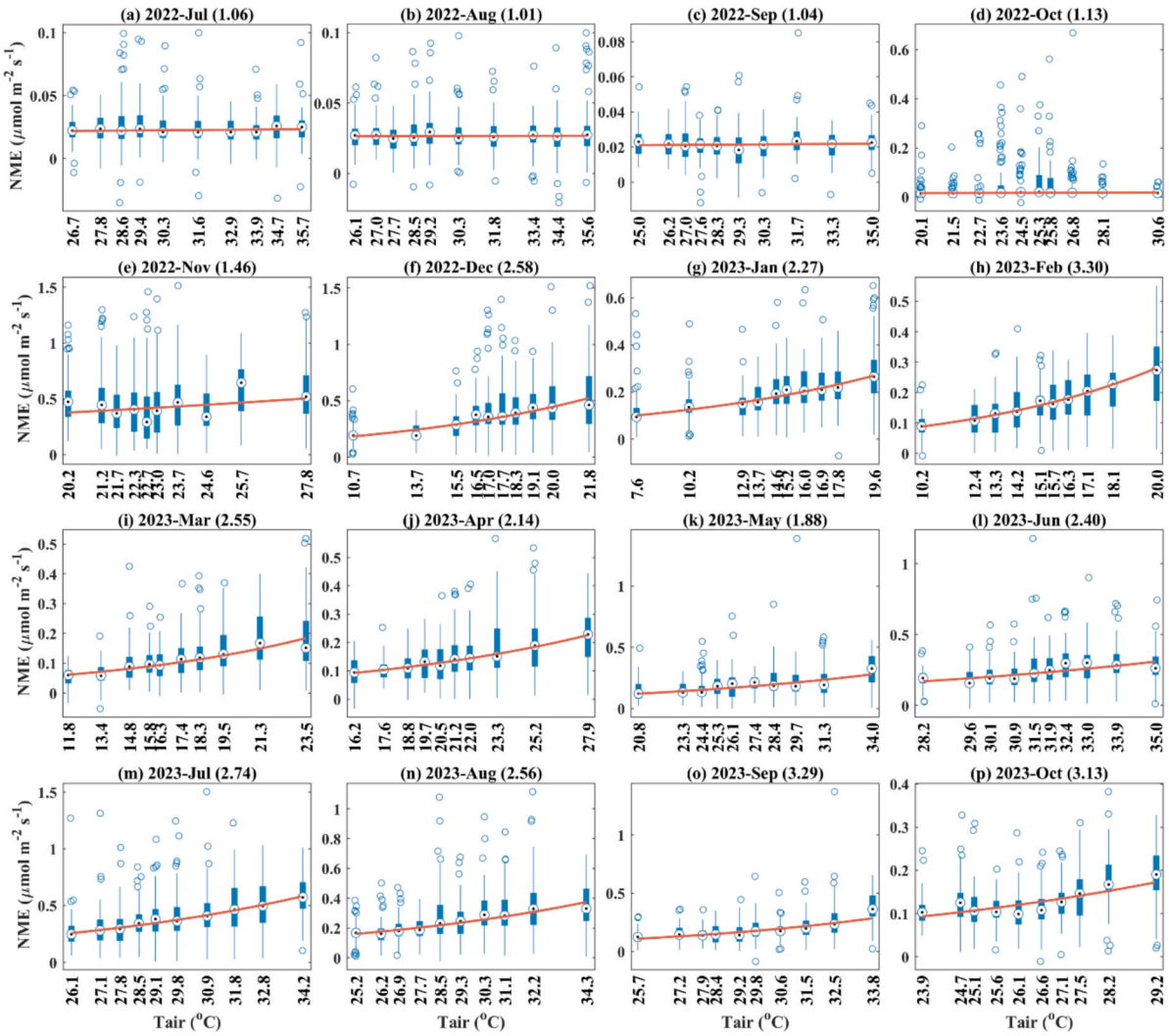

Fig. 6. Response of net methane exchange (NME) to air temperature (Tair) under tidal exposed conditions from Jul. 2022 to Oct. 2023 in a disturbed tidal wetland experiencing smooth cordgrass removals. All 30-min NME data acquired under exposed conditions for each month are bin-averaged into 10 groups by the percentiles of Tair in that month, and then an exponential response function is applied to fit the binned median NME and corresponding percentiles of Tair, as shown on each X-axis. The number in brackets in the sub-title denotes the Q_{10} value of each month. Note that both the X-axis and Y-axis for each month use different scales.

same months (Jul., Aug., and Sep.) between pre- and post-removal periods, the post-removal Q_{10} values were 2.53–3.16 times that of the pre-removal levels. Over the studying period, there was an overall statistically positive relationship between Q_{10} and NME on a monthly scale ($y = 0.026exp^{0.83x}$, $R^2 = 0.44$) (Fig. 7).

4. Discussion

4.1. Changing methane emission with the removal

Previous studies have found that the cordgrass invasion enhances CH_4 emission by altering vegetation productivity, soil properties, and microbial community structure, as well as the characteristics of plant-mediated CH_4 transport, thereby profoundly impacting the soil carbon cycling in coastal wetlands (Yuan et al., 2015; Bu et al., 2019; Liu et al., 2022; Zheng et al., 2023). Similarly, we find the CH_4 fluxes observed in this saltmarsh with invasive cordgrass, ranging from 466.9 to 4203.7 μmol CH_4 m^{-2} d^{-1} before the removal, are significantly higher than the average value of the saltmarsh (224.4 μmol CH_4 m^{-2} d^{-1}) reported by a synthesis study (Al-Haj and Fulweiler, 2020). Given that mowing combined with mechanical plowing is used in the cordgrass removal, the pulse CH_4 emission following the removals can be explained by several aspects. First, the large amount of fragmented plant residues buried by plowing provides abundant fresh carbon substrates for methanogens (Yang et al., 2021), which is similar to the effect of straw incorporation (Zhang et al., 2015). Second, the mechanical soil disturbance and residue decomposition alter microbial community composition (Wang et al., 2023b), favoring fast-growing decomposers that accelerate organic matter breakdown and methanogenic activity (Li et al., 2022). Third, the soil compaction from heavy machinery can form a more stable and anoxic environment that greatly facilitates the methanogenesis (Villa, 2020).

There is a clear positive correlation between the labile organic matter and CH_4 production (Bastviken et al., 2023). Studies have shown that the litter of cordgrass primarily consists of labile organic matter that is easily decomposed (Li et al., 2024; Huang et al., 2025). Mowing and plowing result in a substantial short-term input of the labile organic matter into the soil and thus greatly stimulate CH_4 production and emission. In this study, CH_4 efflux is maintained at high levels for two months after the cordgrass removal, and then gradually decline and stabilize likely due to the exhaustion of the pulse input of labile organic matter (Fig. 2). Although the peak value of second pulse emission in Jul. 2023 is lower than that of first pulse emission, the CH_4 fluxes following the moderate removal remain markedly higher than the same months of

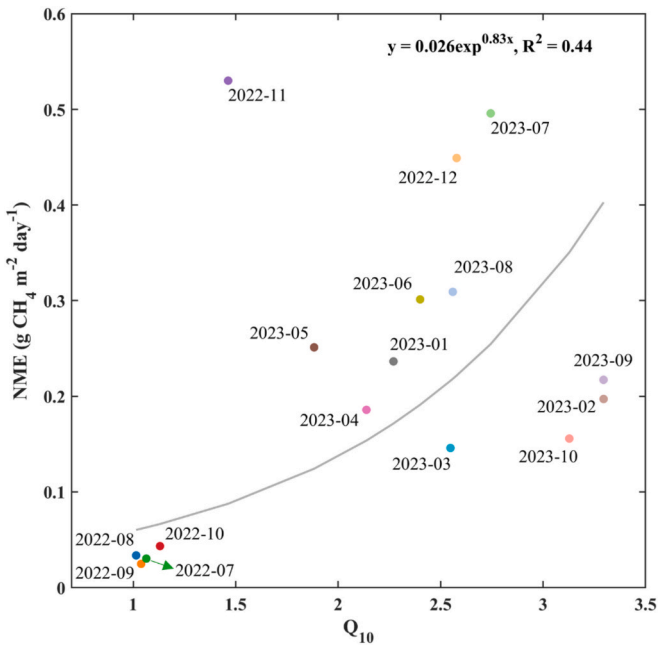

Fig. 7. Response of monthly mean net methane exchange (NME) to its temperature sensitivity (Q_{10}) from Jul. 2022 to Oct. 2023 in a disturbed tidal wetland experiencing smooth cordgrass removals, shown with a fitted exponential response curve.

the previous year. These findings suggest that the substrate availability may be the key determinant of the magnitude and duration of CH_4 pulses. The finding of large changes in the magnitude and temporal variability of CH_4 emission implies that these anthropogenic disturbances may potentially lead to a regime shift in soil CH_4 biogeochemistry. Given that this restoration also causes a large change in CO_2 flux (Zhu et al., 2024b), we also conduct a comparative analysis, using the data within the same time window (Jul. 8th ~ Oct. 20th) before and after the removal, to further examine how the combined effects on both CH_4 and CO_2 fluxes determine the net climate benefit (Fig S1). The comparison reveals that the estimated net climate benefit, based on the sustained-flux global warming potentials metric for a 100-year time horizon (Zhu et al., 2025), changes from a pre-removal cooling effect (-12.03 ± 6.36 g CO_2 eq. m^{-1} day^{-1}) to a post-removal warming effect (15.26 ± 6.23 g CO_2 eq. m^{-1} day^{-1}). It is evident that the combination of the CH_4 pulse emission and the reversal of CO_2 flux leads to a significant negative climate benefit.

4.2. Enlarged tidal impacts on methane emission

Tidal activity is an important factor influencing carbon exchange in BCEs. As a result of the suppressing effects of tidal inundation, the CH_4 fluxes during tidal inundation in this study are significantly lower than those during tidal exposure (Fig. 3). On the one hand, tidal inundation alters soil redox potential and creates a suitable anaerobic environment conducive to CH_4 production while simultaneously constraining CH_4 oxidation. Tidal inundation may also introduce more sediment inputs, indirectly enhancing methane generation (Cui et al., 2024). On the other hand, a large portion of the produced CH_4 diffuses into porewater or overlying water (Hu et al., 2020). Tidal inundation just acts as a physical barrier and inhibiting the release of CH_4 to the atmosphere (Wei et al., 2020), leading to short-term CH_4 accumulation during tidal inundation and pulse emission during tidal exposure (Fig. 5). Additionally, due to tidally driven pore water exchange, the dissolved carbon released from the cordgrass residues are transported laterally into adjacent tidal creeks (Capooci et al., 2024; Huang et al., 2025), where they may be remineralized into CH_4 and emitted into the atmosphere within a short period of time (Bogard et al., 2020). This is likely an additional contributor to the pulse CH_4 emission (Rosentreter et al., 2018).

Tidal pumping is a tidally driven exchange process between porewater and surface water, which significantly influences GHG emissions at the water–air interface in BCEs (Call et al., 2015; Chen et al., 2021a). Such CH_4 emission hotspots induced by tidal pumping have been widely reported in various BCEs, including mangroves and salt marshes (Li et al., 2018; Rosentreter et al., 2018; Zhu et al., 2024a). Over the post-removal period, with little plant-mediated transport through aerenchyma, CH_4 emission primarily occurs via diffusion and ebullition. During ebb tide, the reduction in hydrostatic pressure facilitates the release of CH_4 supersaturated in porewater (Rosenqvist et al., 2002). In the absence of plant-mediated transport, CH_4 accumulated in porewater tends to release rapidly as bubbles, minimizing the oxidative loss of CH_4 during the transport process (Bastviken et al., 2023). Thus, ebullition may be the dominant pathway for CH_4 pulse emission following cordgrass removal. Although the aerenchyma of cordgrass plays a crucial role in CH_4 transport (Comer-Warner et al., 2022), the contribution of ebullition cannot be overlooked, especially under conditions of abundant organic matter (e.g., decaying plant residues) (Bastviken et al., 2023). Notably, tidal inundation and pumping effects occur both before and after the removal, but the difference in CH_4 fluxes between inundated and exposed conditions is significantly greater during the post-removal period. These findings suggest that the removals strengthen tidal controls on CH_4 emission and its diel variability by enhanced tidal inundation and priming effects.

4.3. Enhanced temperature sensitivity of methane emission

It is assumed in this study that the change in organic substrates after the removal is a key factor contributing to the enhanced temperature sensitivity. The Q_{10} value could be affected by the quality and quantity of organic substrates. This explanation is consistent with previous studies that emphasize the critical role of soil substrate availability in modulating the temperature sensitivity of CH_4 emission. An abrupt increase in substrate availability can lead to a higher apparent temperature sensitivity. For instance, Chang et al. (2019) demonstrate that increased labile substrates following peatland thawing heighten CH_4 temperature sensitivity, and Wang et al. (2021) indicate that typhoon and rainstorm events deliver more terrestrial organic matter to wetlands and thus stimulate CH_4 emission. Water table fluctuations in wetland can also modulate the temperature sensitivity by regulating the substrate accessibility and microbial activity (Chen et al., 2021b; Li et al., 2023; Hu et al., 2024). Moreover, experimental evidence reveals that increased carbon availability exerts more positive impacts on the temperature sensitivity of methanogenesis compared to CH_4 oxidation (Inglett et al., 2012). It is possible that the pulse of nutrients released during the decay of cordgrass promotes the establishment of methanogenesis-related microbial communities (Wang et al., 2023b), which not only accelerate methanogenesis but also contribute to a more sensitive temperature response of CH_4 production.

Another possible reason for the enhanced temperature sensitivity is that the cordgrass removal reduces the oxygen availability and thus CH_4 oxidation, leading to a net increase in CH_4 emission. Over the pre-removal period, the diel variation in CH_4 emission is relatively small (Figs. 2a and 3), which is in contrast with the CH_4 flux patterns observed in adjacent mangrove ecosystems (Zhu et al., 2024a). This is likely explained by the fact that daytime CH_4 fluxes are suppressed due to enhanced rhizosphere CH_4 oxidation driven by plant-mediated oxygen transport (Noyce et al., 2023). This explanation is supported by Pearson correlation analyses, showing that the relationship between CH_4 fluxes and PAR reversed from a significant negative correlation before the removal to a significant positive correlation after the removal (Fig. 4). Higher daytime temperature promotes both CH_4 production and oxidation, and thus there is a possibility of no distinct diel variations in net CH_4 emission over the pre-removal period. However, over the post-

removal period, the proportion of daytime CH_4 oxidation could decrease due to lower oxygen supply to the rhizosphere, which leads to an increase in the diel variability of CH_4 emission since higher daytime temperature can significantly stimulate the substrate-rich methanogenesis (Knox et al., 2021).

4.4. Limitations and implications

This study employs the EC technique to monitor the changes in CH_4 fluxes before and after the removal of cordgrass. However, several limitations remain in this study. First, although the EC technique provides high-frequency flux measurements, the data inevitably suffer from uncertainties due to the necessary quality controls and aggregation procedures. To reduce the uncertainty, we apply separate quality control for daytime and nighttime data before aggregating them to daily and monthly scales, which is more methodologically sound (Zhu and Zhu, 2025). Second, although the time-varying footprint coverage may influence the temporal dynamics of NME, our previous study has demonstrated that there is not much difference in footprint climatology during the study period with low coverage of newly established mangroves (Zhu et al., 2024b). Thus, the uncertainty from time-varying footprint coverage should be relatively small. Third, we use the air temperature as a surrogate for soil temperature due to the lack of soil temperature measurements in this study, which may introduce additional uncertainty due to the difference in magnitude and timing between air and soil temperature (Zhu et al., 2024a). Fourthly, we only apply a simple temperature-emission exponential function to examine the temperature sensitivity of CH_4 emission, despite that multiple factors, including temperature, microbial activity, and substrate availability actually influence the emission. Thus, empirical model parameters from these simple fits may not fully reflect the temperature sensitivity of observed flux dynamics (Wang et al., 2015). Fifthly, in addition to the removal activities, the difference in climate conditions between the pre- and post-removal years also affects the interannual variations in observed CH_4 fluxes. Following Zhu et al. (2024b), we partition the removal- and climate-induced contribution (Fig S2) and confirm that the change in CH_4 fluxes is predominantly attributed to the cordgrass removal instead of the climatic difference. Sixthly, although the high-frequency time series of observed CH_4 fluxes confirm that the cordgrass removals trigger CH_4 pulse emissions, our observations covering a one-year post-removal period are not long enough. Future longer flux measurements with extended years are needed to comprehensively assess the long-term evolution of CH_4 fluxes following the removals. Finally, given that the restoration-induced impacts on CH_4 emission depend on the disturbance types, vegetation composition, and environmental conditions, our findings may not be directly extrapolated to other restoration scenarios.

This study confirms the enhancements of both the magnitude and diel variability of CH_4 emission following the cordgrass removal. The disturbance-induced pulse emissions with high diel variability suggest that traditional chamber-based low-frequency measurements cannot well track the strong temporal dynamics of CH_4 flux following intensive cordgrass removals. This fully underscores the unique advantages of high-frequency and continuous EC measurements in assessing GHG flux changes under anthropogenic disturbances (Macreadie et al., 2021). Under the background of global warming, the increased temperature sensitivity of CH_4 emission post-removal implies that future climate warming may induce more intense CH_4 emission. Notably, cordgrass removal often requires repeated implementation, and the short-term CH_4 emission resulting from such periodic anthropogenic disturbances could create a low-frequency but high-magnitude amplification effect in future carbon budgets. Therefore, it is essential to consider GHG emission throughout the entire land-use change process in ecological restoration projects. This is because such CH_4 pulses of limited duration but considerable intensity pose a significant risk of offsetting the blue carbon benefits brought by ecological restoration.

5. Conclusions

The world's largest coastal ecosystem restoration is being implemented in coastal China to intensively remove invasive smooth cordgrass, potentially exerting a large impact on soil CH_4 emission. To assess the degree to which CH_4 emission and its environmental controls change with such anthropogenic disturbances, we utilize the eddy covariance method to track the temporal variability of CH_4 flux over both pre- and post-removal periods in a disturbed saltmarsh-mangrove wetland of Southeast China. Our high-frequency flux measurements reveal that the removal causes a pulse of CH_4 emission that is about one order of magnitude higher than the pre-removal level. We find that the removal not only intensifies the controls of tidal inundation and pumping on the CH_4 emission, but also enlarges the temperature sensitivity of the CH_4 emission. The combination of enhanced tidal impacts and temperature dependence thus promotes the diel variability of CH_4 flux over the post-removal period. These results highlight the necessity of better understanding the climate impact of restoration activities, which helps close the knowledge gap in assessing restoration-induced environmental risk of greenhouse gas flux changes. Future longer flux data with extended years are needed to further assess potential regime shift in soil CH_4 biogeochemistry and long-term evolution of such unintended environmental costs of the restoration.

CRediT authorship contribution statement

Yueting Deng: Writing – original draft, Visualization, Methodology, Investigation, Formal analysis, Data curation. **Ruichen Lin:** Visualization, Investigation, Data curation. **Han Yang:** Investigation, Data curation. **Hui Luo:** Investigation, Data curation. **Lulu Song:** Writing – review & editing, Supervision, Resources. **Xudong Zhu:** Writing – review & editing, Supervision, Resources, Project administration, Funding acquisition, Conceptualization.

Declaration of competing interest

The authors declare that they have no known competing financial interests or personal relationships that could have appeared to influence the work reported in this paper.

Acknowledgments

We are grateful to the staff at Zhangjiang Estuary Mangrove National Nature Reserve for their help in the fieldwork. This work was jointly supported by Natural Science Foundation of Fujian Province of China (2023J06008), National Natural Science Foundation of China (32371661), National Key Research and Development Program of China (2022YFF0802101, 2024YFF1306805), External Cooperation Program of Fujian Science and Technology Department (2023I0036), the 2023 Google Carbon Removal Research Awards, and the PhD Fellowship & Internal Program (MELRI2601) of the State Key Laboratory of Marine Environmental Science at Xiamen University.

Appendix A. Supplementary data

Supplementary data to this article can be found online at https://doi.org/10.1016/j.geoderma.2026.117719.

Data availability

Data will be made available on request.

References

Al-Haj, A.N., Fulweiler, R.W., 2020. A synthesis of methane emissions from shallow vegetated coastal ecosystems. Glob. Chang. Biol. 26 (5), 2988–3005. https://doi.org/10.1111/gcb.15046.

Baldocchi, D.D., 2020. How eddy covariance flux measurements have contributed to our understanding of Global Change Biology. Glob. Chang. Biol. 26 (1), 242–260. https://doi.org/10.1111/gcb.14807.

Bastviken, D., Treat, C.C., Pangala, S.R., et al., 2023. The importance of plants for methane emission at the ecosystem scale. Aquat. Bot. 184, 103596. https://doi.org/10.1016/j.aquabot.2022.103596.

Bogard, M.J., Bergamaschi, B.A., Butman, D.E., et al., 2020. Hydrologic export is a major component of coastal wetland carbon budgets. Global Biogeochem. Cycles 34 (8), e2019GB006430. https://doi.org/10.1029/2019GB006430.

Bridgham, S.D., Cadillo-Quiroz, H., Keller, J.K., et al., 2013. Methane emissions from wetlands: biogeochemical, microbial, and modeling perspectives from local to global scales. Glob. Chang. Biol. 19, 1325–1346. https://doi.org/10.1111/gcb.12131.

Bu, N., Wu, S., Yang, X., et al., 2019. *Spartina alterniflora* invasion affects methane emissions in the Yangtze River estuary. J. Soil. Sediment. 19 (2), 579–587. https://doi.org/10.1007/s11368-018-2073-5.

Call, M., Maher, D.T., Santos, I.R., et al., 2015. Spatial and temporal variability of carbon dioxide and methane fluxes over semi-diurnal and spring–neap–spring timescales in a mangrove creek. Geochim. Cosmochim. Acta 150, 211–225. https://doi.org/10.1016/j.gca.2014.11.023.

Capooci, M., Seyfferth, A.L., Tobias, C., et al., 2024. High methane concentrations in tidal salt marsh soils: where does the methane go? Glob. Chang. Biol. 30 (1), e17050. https://doi.org/10.1111/gcb.17050.

Chang, K.-Y., Riley, W.J., Brodie, E.L., et al., 2019. Methane production pathway regulated proximally by substrate availability and distally by temperature in a high-latitude mire complex. J. Geophys. Res. Biogeo. 124 (10), 3057–3074. https://doi.org/10.1029/2019JG005355.

Chen, X., Santos, I.R., Call, M., et al., 2021a. The mangrove CO_2 pump: Tidally driven pore-water exchange. Limnol. Oceanogr. 66 (4), 1563–1577. https://doi.org/10.1002/lno.11704.

Chen, H., Xu, X., Fang, C., et al., 2021b. Differences in the temperature dependence of wetland CO_2 and CH_4 emissions vary with water table depth. Nat. Clim. Chang. 11 (9), 766–771. https://doi.org/10.1038/s41558-021-01108-4.

Comer-Warner, S.A., Ullah, S., Ampuero Reyes, W., et al., 2022. *Spartina alterniflora* has the highest methane emissions in a St. Lawrence estuary salt marsh. Environmental Research: Ecology 1 (1), 011003. https://doi.org/10.1088/2752-664X/ac706a.

Cui, S., Liu, P., Guo, H., et al., 2024. Wetland hydrological dynamics and methane emissions. Commun. Earth Environ. 5 (1), 1–17. https://doi.org/10.1038/s43247-024-01635-w.

Deng, Y., Guo, X., Zhao, X., et al., 2025. Coastal macroalgae aquaculture reduces carbon dioxide emission in a subtropical enclosed bay: Insights from eddy covariance measurements. Agr Ecosyst Environ 385, 109576. https://doi.org/10.1016/j.agee.2025.109576.

Fu, C., Steckbauer, A., Mann, H., et al., 2024. Achieving the Kunming–Montreal global biodiversity targets for blue carbon ecosystems. Nature Reviews Earth & Environment 5 (7), 538–552. https://doi.org/10.1038/s43017-024-00566-6.

He, Q., Li, Z., Daleo, P., et al., 2025. Coastal wetland resilience through local, regional and global conservation. Nature Reviews Biodiversity 1 (1), 50–67. https://doi.org/10.1038/s44358-024-00004-x.

Hu, H., Chen, J., Zhou, F., et al., 2024. Relative increases in CH_4 and CO_2 emissions from wetlands under global warming dependent on soil carbon substrates. Nat. Geosci. 17 (1), 26–31. https://doi.org/10.1038/s41561-023-01345-6.

Hu, M., Sardans, J., Yang, X., et al., 2020. Patterns and environmental drivers of greenhouse gas fluxes in the coastal wetlands of China: a systematic review and synthesis. Environ. Res. 186, 109576. https://doi.org/10.1016/j.envres.2020.109576.

Huang, Y., Wang, J., Wu, P., et al., 2025. Impacts of *Spartina alterniflora* invasion on coastal carbon cycling within a native *Phragmites australis*-dominated wetland. Agric. For. Meteorol. 363, 110405. https://doi.org/10.1016/j.agrformet.2025.110405.

Inglett, K.S., Inglett, P.W., Reddy, K.R., et al., 2012. Temperature sensitivity of greenhouse gas production in wetland soils of different vegetation. Biogeochemistry 108, 77–90. https://doi.org/10.1007/s10533-011-9573-3.

Knox, S.H., Bansal, S., McNicol, G., et al., 2021. Identifying dominant environmental predictors of freshwater wetland methane fluxes across diurnal to seasonal time scales. Glob. Chang. Biol. 27 (15), 3582–3604. https://doi.org/10.1111/gcb.15661.

Li, G., Xu, S., Tang, Y., et al., 2024. *Spartina alterniflora* invasion altered soil greenhouse gas emissions via affecting labile organic carbon in a coastal wetland. Appl. Soil Ecol. 203, 105615. https://doi.org/10.1016/j.apsoil.2024.105615.

Li, H., Dai, S., Ouyang, Z., et al., 2018. Multi-scale temporal variation of methane flux and its controls in a subtropical tidal salt marsh in eastern China. Biogeochemistry 137 (1), 163–179. https://doi.org/10.1007/s10533-017-0413-y.

Li, J., Pei, J., Fang, C., et al., 2023. Opposing seasonal temperature dependencies of CO_2 and CH_4 emissions from wetlands. Glob. Chang. Biol. 29 (4), 1133–1143. https://doi.org/10.1111/gcb.16528.

Li, L., Jiang, X., Zhou, Q., et al., 2022. Responses of soil microbiota to different control methods of *the spartina alterniflora* in the Yellow River Delta. Microorganisms 10 (6), 1122. https://doi.org/10.3390/microorganisms10061122.

Liu, J., Wang, W., Shen, L., et al., 2022. Response of methanotrophic activity and community structure to plant invasion in China's coastal wetlands. Geoderma 407, 115569. https://doi.org/10.1016/j.geoderma.2021.115569.

Liu, Y., Zhu, X., 2024. Tracking mangrove light use efficiency using normalized difference red edge index. Ecol. Ind. 168, 112774. https://doi.org/10.1016/j.ecolind.2024.112774.

Liu, Z., Cui, B., He, Q., 2016. Shifting paradigms in coastal restoration: six decades' lessons from China. Sci. Total Environ. 566–567, 205–214. https://doi.org/10.1016/j.scitotenv.2016.05.049.

Lu, Y., Zhu, X., 2021. Response of mangrove carbon fluxes to drought stress detected by photochemical reflectance index. Remote Sens. (Basel) 13 (20), 4053. https://doi.org/10.3390/rs13204053.

Macreadie, P.I., Costa, M.D.P., Atwood, T.B., et al., 2021. Blue carbon as a natural climate solution. Nature Reviews Earth & Environment 2 (12), 826–839. https://doi.org/10.1038/s43017-021-00224-1.

Mauder, M., Cuntz, M., Drüe, C., Graf, A., Rebmann, C., Schmid, H.P., Schmidt, M., Steinbrecher, R., 2013. A strategy for quality and uncertainty assessment of long-term eddy-covariance measurements. Agr. Forest Meteorol. 169, 122–135.

Nie, M., Liu, W., Pennings, S.C., et al., 2023. Lessons from the invasion of *Spartina alterniflora* in coastal China. Ecology 104 (1), e3874.

Noyce, G.L., Megonigal, J.P., 2021. Biogeochemical and plant trait mechanisms drive enhanced methane emissions in response to whole-ecosystem warming. Biogeosciences 18 (8), 2449–2463. https://doi.org/10.5194/bg-18-2449-2021.

Noyce, G.L., Smith, A.J., Kirwan, M.L., et al., 2023. Oxygen priming induced by elevated CO_2 reduces carbon accumulation and methane emissions in coastal wetlands. Nat. Geosci. 16 (1), 63–68. https://doi.org/10.1038/s41561-022-01070-6.

Pendleton, L., Donato, D.C., Murray, B.C., et al., 2012. Estimating global "blue carbon" emissions from conversion and degradation of vegetated coastal ecosystems. PLoS One 7 (9), e43542. https://doi.org/10.1371/journal.pone.0043542.

Qi, G., Li, L., Li, H., et al., 2024. Ecological effects of the huge invasive species removal project in coastal China. Environ. Sci. Technol. 58 (48), 21229–21241. https://doi.org/10.1021/acs.est.4c05253.

Rosenqvist, Å., Forsberg, B.R., Pimentel, T., et al., 2002. The use of spaceborne radar data to model inundation patterns and trace gas emissions in the central Amazon floodplain. Int. J. Remote Sens. 23 (7), 1303–1328. https://doi.org/10.1080/01431160110092911.

Rosentreter, J.A., Laruelle, G.G., Bange, H.W., et al., 2023. Coastal vegetation and estuaries are collectively a greenhouse gas sink. Nat. Clim. Chang. 13 (6), 579–587. https://doi.org/10.1038/s41558-023-01682-9.

Rosentreter, J.A., Maher, D.T., Erler, D.V., et al., 2018. Methane emissions partially offset "blue carbon" burial in mangroves. Sci. Adv. 4 (6), eaao4985. https://doi.org/10.1126/sciadv.aao4985.

Sasmito, S.D., Taillardat, P., Clendenning, J.N., et al., 2019. Effect of land-use and land-cover change on mangrove blue carbon: a systematic review. Glob. Chang. Biol. 25 (12), 4291–4302. https://doi.org/10.1111/gcb.14774.

Stokstad, E., 2023. China battles alien weed at unprecedented scale. Science 379, 972. https://doi.org/10.1126/science.adh4966.

Villa, J.A., 2020. Functional representation of biological components in methane-cycling processes in wetlands improves modeling predictions. J. Geophys. Res. Biogeo. 125 (10), e2020JG005794. https://doi.org/10.1029/2020JG005794.

Wang, C., Lai, D.Y.F., Tong, C., et al., 2015. Variations in temperature sensitivity (Q_{10}) of CH_4 emission from a subtropical estuarine marsh in southeast China. PLoS One 10 (5), e0125227. https://doi.org/10.1371/journal.pone.0125227.

Wang, F., Liu, J., Qin, G., et al., 2023a. Coastal blue carbon in China as a nature-based solution toward carbon neutrality. The Innovation 4 (5), 100481. https://doi.org/10.1016/j.xinn.2023.100481.

Wang, C., Sardans, J., Tong, C., et al., 2021. Typhoon-induced increases in porewater nutrient concentrations and CO_2 and CH_4 emissions associated with salinity and carbon intrusion in a subtropical tidal wetland in China: a mesocosm study. Geoderma 384, 114800. https://doi.org/10.1016/j.geoderma.2020.114800.

Wang, K., Wang, S., Zhang, X., et al., 2023b. Potential ecological impacts of physical control on *Spartina alterniflora* in coastal wetland: Migration and transformation of nutrients and the response of bacterial community structure. J. Clean. Prod. 398, 136556. https://doi.org/10.1016/j.jclepro.2023.136556.

Wang, X., Zhu, X., 2024. Salinity stress and atmospheric dryness co-limit evapotranspiration in a subtropical monsoonal estuarine mangrove wetland. Environ. Res. Lett. 19, 114067. https://doi.org/10.1088/1748-9326/ad8586.

Wei, S., Han, G., Chu, X., et al., 2020. Effect of tidal flooding on ecosystem CO_2 and CH_4 fluxes in a salt marsh in the Yellow River Delta. Estuar. Coast. Shelf Sci. 232, 106512. https://doi.org/10.1016/j.ecss.2019.106512.

Xie, B., Han, G., 2023. Control of invasive plant *Spartina alterniflora*: Concept, technology and practice. Bulletin of Chinese Academy of Sciences (chinese Version) 38 (12), 1924–1938. https://doi.org/10.16418/j.issn.1000-3045.20230921001.

Yang, B., Li, X., Lin, S., et al., 2021. Invasive *Spartina alterniflora* changes the Yangtze Estuary salt marsh from CH_4 sink to source. Estuar. Coast. Shelf Sci. 252, 107258. https://doi.org/10.1016/j.ecss.2021.107258.

Yang, L., Chi, Y., Lu, H., et al., 2024. Effects of the comprehensive elimination of *Spartina alterniflora* along China's coast on blue carbon and scenario prediction after ecological restoration. J. Environ. Manage. 369, 122283. https://doi.org/10.1016/j.jenvman.2024.122283.

Yuan, J., Ding, W., Liu, D., et al., 2015. Exotic *Spartina alterniflora* invasion alters ecosystem–atmosphere exchange of CH_4 and N_2O and carbon sequestration in a coastal salt marsh in China. Glob. Chang. Biol. 21 (4), 1567–1580. https://doi.org/10.1111/gcb.12797.

Zhang, L., Zheng, J., Chen, L., et al., 2015. Integrative effects of soil tillage and straw management on crop yields and greenhouse gas emissions in a rice–wheat cropping system. Eur. J. Agron. 63, 47–54. https://doi.org/10.1016/j.eja.2014.11.005.

Zhang, Y., Guo, X., Zhu, X., 2023. Strong diurnal variability of carbon dioxide flux over algae-shellfish aquaculture ponds revealed by eddy covariance measurements. Agr Ecosyst Environ 348, 108426. https://doi.org/10.1016/j.agee.2023.108426.

Zhang, Y., Qin, Z., Li, T., et al., 2022. Carbon dioxide uptake overrides methane emission at the air-water interface of algae-shellfish mariculture ponds: evidence from eddy covariance observations. Sci. Total Environ. 815, 152867. https://doi.org/10.1016/j.scitotenv.2021.152867.

Zheng, X., Javed, Z., Liu, B., et al., 2023. Impact of *Spartina alterniflora* invasion in coastal wetlands of China: boon or bane? Biology 12 (8), 1057. https://doi.org/10.3390/biology12081057.

Zhu, X., Chen, J., Li, L., et al., 2024a. Asynchronous methane and carbon dioxide fluxes drive temporal variability of mangrove blue carbon sequestration. Geophysical Research Letters 51(11), e2023GL107235. doi:10.1029/2023GL107235.

Zhu, X., Hou, Y., Zhang, Y., et al., 2021a. Potential of sun-induced chlorophyll fluorescence for indicating mangrove canopy photosynthesis. Journal of Geophysical Research: Biogeosciences 126, e2020JG006159. doi:10.1029/2020JG006159.

Zhu, X., Hou, Y., Weng, Q., et al., 2019a. Integrating UAV optical imagery and LiDAR data for assessing the spatial relationship between mangrove and inundation across a subtropical estuarine wetland. ISPRS J. Photogramm. Remote Sens. 149, 146–156. https://doi.org/10.1016/j.isprsjprs.2019.01.021.

Zhu, X., Ma, M., Li, L., et al., 2024b. Impacts of intensive smooth cordgrass removal on net ecosystem exchange in a saltmarsh-mangrove ecotone of Southeast China. Sci. Total Environ. 934, 173202. https://doi.org/10.1016/j.scitotenv.2024.173202.

Zhu, X., Meng, L., Zhang, Y., et al., 2019b. Tidal and meteorological influences on the growth of invasive *spartina alterniflora*: evidence from UAV remote sensing. Remote Sens. (Basel) 11 (10), 1208. https://doi.org/10.3390/rs11101208.

Zhu, X., Qin, Z., Liu, W., et al., 2025. Coastal restoration may not necessarily enhance blue carbon sink. Geophys. Res. Lett. 52, e2025GL114614. https://doi.org/10.1029/2025GL114614.

Zhu, X., Qin, Z., Song, L., 2021b. How land-sea interaction of tidal and sea breeze activity affect mangrove net ecosystem exchange? J. Geophys. Res. Atmos. 126 (8), e2020JD034047. https://doi.org/10.1029/2020JD034047.

Zhu, X., Song, L., Weng, Q., et al., 2019c. Linking in situ photochemical reflectance index measurements with mangrove carbon dynamics in a subtropical coastal wetland. J. Geophys. Res. Biogeo. 124, 1714–1730. https://doi.org/10.1029/2019JG005022.

Zhu, X., Sun, C., Qin, Z., 2021c. Drought-induced salinity enhancement weakens mangrove greenhouse gas cycling. J. Geophys. Res. Biogeo. 126, e2021JG006416. https://doi.org/10.1029/2021JG006416.

Zhu, Z., Zhu, X., 2025. Increasing midday depression of mangrove photosynthesis with heat and drought stresses. Agric. For. Meteorol. 362, 110372. https://doi.org/10.1016/j.agrformet.2024.110372.